International Journal of Numerical Methods for Heat & Fluid Flow

Turbulent natural convection combined with surface thermal radiation in a square cavity with local heater

Igor Miroshnichenko, Mikhail Sheremet, Ali J. Chamkha,

Received 5 March 2018
Revised 30 April 2018
Accepted 2 May 2018

Turbulent natural convection combined with surface thermal radiation in a square cavity with local heater

Igor Miroshnichenko and Mikhail Sheremet
Laboratory on Convective Heat and Mass Transfer, Tomsk State University, Tomsk, Russia, and

Ali J. Chamkha
Department of Mechanical Engineering, Prince Sultan Endowment for Energy and Environment, Prince Mohammad Bin Fahd University, Al-Khobar, Saudi Arabia and Rak Research and Innovation Center, American University of Ras Al Khaimah, Ras Al Khaimah, United Arab Emirates

Abstract

Purpose – The purpose of this paper is to conduct a numerical analysis of transient turbulent natural convection combined with surface thermal radiation in a square cavity with a local heater.

Design/methodology/approach – The domain of interest includes the air-filled cavity with cold vertical walls, adiabatic horizontal walls and isothermal heater located on the bottom cavity wall. It is assumed in the analysis that the thermophysical properties of the fluid are independent of temperature and the flow is turbulent. Surface thermal radiation is considered for more accurate analysis of the complex heat transfer inside the cavity. The governing equations have been discretized using the finite difference method with the non-uniform grid on the basis of the special algebraic transformation. Turbulence was modeled using the k–ε model. Simulations have been carried out for different values of the Rayleigh number, surface emissivity and location of the heater.

Findings – It has been found that the presence of surface radiation leads to both an increase in the average total Nusselt number and intensive cooling of such type of system. A significant intensification of convective flow was also observed owing to an increase in the Rayleigh number. It should be noted that a displacement of the heater from central part of the bottom wall leads to significant modification of the thermal plume and flow pattern inside the cavity.

Originality/value – An efficient numerical technique has been developed to solve this problem. The originality of this work is to analyze unsteady turbulent natural convection combined with surface thermal radiation in a square air-filled cavity in the presence of a local isothermal heater. The results would benefit scientists and engineers to become familiar with the analysis of turbulent convective–radiative heat transfer in enclosures with local heaters, and the way to predict the heat transfer rate in advanced technical systems, in industrial sectors including transportation, power generation, chemical sectors and electronics.

Keywords Heat source, Numerical results, Finite difference method, Turbulent natural convection, Surface thermal radiation

Paper type Research paper

International Journal of Numerical Methods for Heat & Fluid Flow
Vol. 28 No. 7, 2018
pp. 1698-1715

0961-5539
DOI 10.1108/HFF-03-2018-0089

This work was supported by the Russian Science Foundation (Project No. 17-79-20141).

Nomenclature

E = dimensionless dissipation rate of turbulent kinetic energy;

F_{k-i} = view factor from k-th element to the i-th element of an enclosure;

g = acceleration of gravity;

G_k = dimensionless generation/destruction of buoyancy turbulent kinetic energy;

k = dimensional turbulent kinetic energy;

K = dimensionless turbulent kinetic energy;

L = size of an air cavity;

$\mathrm{N_{rad}} = \sigma T_h^4 L/[\lambda\,(T_h - T_c)]$ = radiation number;

$\mathrm{Nu_{con}} = \int_0^1 \left|\frac{\partial \Theta}{\partial X}\right|_{X=0} dY$ = average convective Nusselt number;

$\mathrm{Nu_{rad}} = \mathrm{N_{rad}} \int_0^1 Q_{\mathrm{rad}}\Big|_{X=0} dY$ = average radiative Nusselt number;

$\tilde{P}_k$ = dimensionless shearing production;

$Pr = \nu/\alpha$ = Prandtl number;

$Pr = \nu_t/\alpha_t$ = turbulent Prandtl number;

Q_{rad} = dimensionless net radiative heat flux;

R_k = dimensionless radiosity of the k-th element of an enclosure;

$Ra = g\beta\,(T_h - T_c)L^3/(\nu\alpha)$ = Rayleigh number;

t = time;

T = temperature;

T_c = cold wall temperature;

T_h = heat source temperature;

u, v = dimensional velocity components in x and y directions;

U, V = dimensionless velocity components in X and Y directions;

x, y = dimensional Cartesian coordinates; and

X, Y = dimensionless Cartesian coordinates.

Greek symbols

α = air thermal diffusivity;

α_t = turbulent thermal diffusivity;

β = coefficient of volumetric thermal expansion;

ε = dimensional dissipation rate of turbulent kinetic energy;

$\tilde{\varepsilon}$ = surface emissivity;

Θ = dimensionless temperature;

λ = thermal conductivity;

ν = kinematic viscosity;

ν_t = turbulent viscosity;

$\zeta = T_c/T_h$ = temperature parameter;

ρ = density;

κ = compaction parameter;

σ = Stefan-Boltzmann constant;

τ = dimensionless time;

ψ = dimensional stream function;

Ψ = dimensionless stream function;

ω = dimensional vorticity;
Ω = dimensionless vorticity; and
ξ, η = new dimensionless independent variables.

1. Introduction

Experimental and numerical studies of turbulent natural convection coupled with radiation heat transfer in enclosures have become interesting for researchers in the field of fluid mechanics and heat transfer. The interest in this problem is because of the importance of these processes in numerous engineering applications, such as thermal comfort in building (Jaluria, 1998). Although many detailed studies have been carried out in this area (Jaluria, 1998; Sharma *et al.*, 2007; Shati *et al.*, 2013; Xaman *et al.*, 2008; Ibrahim *et al.*, 2013; Miroshnichenko and Sheremet, 2015; Sheremet and Miroshnichenko, 2016), these processes are not fully understood and they are still of significant interest. Thus, Fusegi and Farouk (1989) presented a numerical investigation of laminar and turbulent natural convection and thermal radiation in differentially heated square enclosures. They found that a presence of radiation changes significantly the characteristics of flow and temperature fields within the cavity under the thermal boundary conditions considered. Furthermore, thermal surface radiation causes hydrodynamic and thermal boundary layers to be thickened. Colomer *et al.* (2004) studied the phenomenon of radiation and natural convection in a three-dimensional cavity using the discrete ordinates method. The effect of the Planck number on the heat flux for different values of the Rayleigh number was investigated in their work. The interaction of thermal surface radiation and laminar natural convection in parabolic enclosure was analyzed by Diaz and Winston (2008) using the finite difference method. Obtained results show that emissivity has a strong effect on the average radiative Nusselt number especially at high Rayleigh numbers. Recently, Wu and Lei (2015) compared the experimental and numerical results for turbulent natural convection and radiation in a differentially heated cavity without heat source.

Natural convection in enclosures with a heat source has also attracted a lot of attention. Sezai and Mohamad (2000) performed three-dimensional numerical simulation of natural convection in an enclosure with a heat source. The effects of the Rayleigh number and aspect ratio of the source on the Nusselt number were investigated in their work. Furthermore, they concluded that the edge effects decrease with the growth of the heater length. Paroncini and Corvaro (2009) experimentally and numerically investigated the convective heat transfer generated by a source with three different heights. They found that the heat transfer by natural convection worsens with the increase in the source height. Martyushev and Sheremet (2014a, 2014b) investigated free convection combined with thermal surface radiation in a cavity bounded by heat-conducting solid walls in the presence of a heat source of constant temperature in two-dimensional (Martyushev and Sheremet, 2014a) and three-dimensional (Martyushev and Sheremet, 2014b) cases. It has been shown that surface emissivity and local heat source have an essential influence of the heat transfer rate.

A lot of theoretical studies of natural convection and thermal surface radiation in an enclosure containing a discrete heater at its center have been done (Saravanan and Sivaraj, 2014; Sun *et al.*, 2011; Mezrhab *et al.*, 2006). There is still lacking information about the influence of heat source size and location on fluid flow and heat transfer characteristics. The numerical study of two-dimensional laminar natural convection with surface radiation in open top cavity with a heat source has been performed by Singh and Singh (2015). They found an optimal location of heat source for efficient cooling of the analyzed system. The effect of heater aspect ratio on free convection in a rectangular enclosure was studied

experimentally and numerically by Biswas *et al.* (2016). They found that the Prandtl and Rayleigh numbers and heater sizes have strong influence on the flow pattern and entropy production rate inside the cavity.

Combined with our observations from a thorough review of the literature, the effect of heat source location on turbulent natural convection with thermal surface radiation in enclosure has been investigated in a very few studies. It is observed that in applications associated with large enclosures, Rayleigh number is frequently very high, meaning that the nature of convection in the enclosure is fully turbulent. So, the main aim of the present study is to numerically assess the influence of Rayleigh number, surface emissivity and heater location on fluid flow field, temperature distributions and average Nusselt number.

2. Physical and mathematical models

The two-dimensional unsteady turbulent natural convection with surface thermal radiation in a square enclosure with a local heat source is considered using the system of coordinates as shown in Figure 1. Here, L represents the width and height of the enclosure. The discrete heater is assumed to be isothermal at a higher temperature T_h, while the vertical walls are maintained at low temperature T_c. The horizontal walls are considered to be adiabatic. The surfaces are supposed to be gray and diffuse, and thermophysical properties of the fluid are constant. The medium under consideration is air, which is both radiatively transparent and incompressible, and also Boussinesq approximation is valid.

Based on the above assumptions, the process of heat transfer in considered area has been governed by the system of unsteady turbulent natural convection equations in two-dimensional air-filled cavity (Miroshnichenko and Sheremet, 2015; Sheremet and Miroshnichenko, 2016). The turbulence effects on the fluid flow and heat transfer are taken into account using the standard $k-\varepsilon$ model (Miroshnichenko and Sheremet, 2015; Sheremet and Miroshnichenko, 2016; Launder and Spalding, 1974). For this problem, it is convenient to write the partial differential equations in dimensionless form with following dimensionless variables:

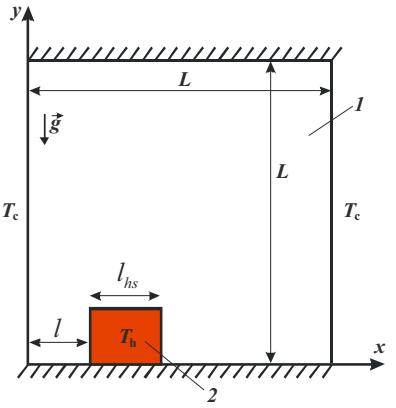

Note: 1 – air, 2 – heat source of constant temperature

Figure 1.
The domain of interest

$$X = x/L,\ Y = y/L,\ \tau = t\sqrt{g\beta\Delta T/L},\ U = u/\sqrt{g\beta\Delta TL},\ V = v/\sqrt{g\beta\Delta TL},$$

$$\Theta = (T - T_0)/\Delta T,\ \Psi = \psi/\sqrt{g\beta\Delta TL^3},\ \Omega = \omega\sqrt{L/g\beta\Delta T},\ K = k/(g\beta\Delta TL),$$

$$E = \varepsilon/\sqrt{g^3\beta^3(\Delta T)^3L},\ T_0 = 0.5(T_c + T_h)$$

Taking into account these variables, the governing equations can be written as follows:

$$\frac{\partial^2\Psi}{\partial X^2} + \frac{\partial^2\Psi}{\partial Y^2} = -\Omega \tag{1}$$

$$\frac{\partial\Omega}{\partial\tau} + \left(U - \frac{\partial\nu_t}{\partial X}\right)\frac{\partial\Omega}{\partial X} + \left(U - \frac{\partial\nu_t}{\partial Y}\right)\frac{\partial\Omega}{\partial Y} = \frac{\partial}{\partial X}\left[\left(\sqrt{\frac{Pr}{Ra}} + \nu_t\right)\frac{\partial\Omega}{\partial X}\right]$$
$$+ \frac{\partial}{\partial Y}\left[\left(\sqrt{\frac{Pr}{Ra}} + \nu_t\right)\frac{\partial\Omega}{\partial Y}\right] + \left(\frac{\partial^2\nu_t}{\partial X^2} - \frac{\partial^2\nu_t}{\partial Y^2}\right)\left(\Omega + 2\frac{\partial U}{\partial Y}\right) + 4\frac{\partial^2\nu_t}{\partial X\partial Y}\frac{\partial V}{\partial Y} + \frac{\partial\Theta}{\partial X} \tag{2}$$

$$\frac{\partial\Theta}{\partial\tau} + U\frac{\partial\Theta}{\partial X} + V\frac{\partial\Theta}{\partial Y} = \frac{\partial}{\partial X}\left[\left(\frac{1}{\sqrt{Ra\cdot\mathrm{Pr}}} + \frac{\nu_t}{\mathrm{Pr}_t}\right)\frac{\partial\Theta}{\partial X}\right] + \frac{\partial}{\partial Y}\left[\left(\frac{1}{\sqrt{Ra\cdot\mathrm{Pr}}} + \frac{\nu_t}{\mathrm{Pr}_t}\right)\frac{\partial\Theta}{\partial Y}\right] \tag{3}$$

$$\frac{\partial K}{\partial\tau} + U\frac{\partial K}{\partial X} + V\frac{\partial K}{\partial Y} = \frac{\partial}{\partial X}\left[\left(\sqrt{\frac{Pr}{Ra}} + \frac{\nu_t}{\sigma_k}\right)\frac{\partial K}{\partial X}\right]$$
$$+ \frac{\partial}{\partial Y}\left[\left(\sqrt{\frac{Pr}{Ra}} + \frac{\nu_t}{\sigma_k}\right)\frac{\partial K}{\partial Y}\right] + \tilde{P}_k + \tilde{G}_k - E \tag{4}$$

$$\frac{\partial E}{\partial\tau} + U\frac{\partial E}{\partial X} + V\frac{\partial E}{\partial Y} = \frac{\partial}{\partial X}\left[\left(\sqrt{\frac{Pr}{Ra}} + \frac{\nu_t}{\sigma_\varepsilon}\right)\frac{\partial E}{\partial X}\right] + \frac{\partial}{\partial Y}\left[\left(\sqrt{\frac{Pr}{Ra}} + \frac{\nu_t}{\sigma_\varepsilon}\right)\frac{\partial E}{\partial Y}\right]$$
$$+ c_{1\varepsilon}(\tilde{P}_k + c_{3\varepsilon}\tilde{G}_k)\frac{E}{K} - c_{2\varepsilon}\frac{E^2}{K} \tag{5}$$

For the model adopted in this study, the production terms for turbulent kinetic energy include shearing production $\tilde{P}_k = \nu_t\left[2\left(\frac{\partial U}{\partial X}\right)^2 + 2\left(\frac{\partial V}{\partial Y}\right)^2 + \left(\frac{\partial U}{\partial Y} + \frac{\partial V}{\partial X}\right)^2\right]$ and generation/destruction of buoyancy turbulent kinetic energy $\tilde{G}_k = -\frac{\nu_t}{\mathrm{Pr}_t}\frac{\partial\Theta}{\partial Y}$ with turbulent kinematic viscosity $\nu_t = c_\mu\frac{K^2}{E}$.

The values of the governing turbulent parameters recommended by Miroshnichenko and Sheremet (2015), Sheremet and Miroshnichenko (2016), Launder and Spalding (1974) and

Sheremet and Miroshnichenko (2015) can be presented in the following form: $\tilde{c}_{\mu} = 0.0$, $\tilde{c}_{1\varepsilon} = 1.44, \tilde{c}_{2\varepsilon} = 1.92, \tilde{c}_{3\varepsilon} = 0.8, \mathrm{Pr}_t = 1.0, \sigma_k = 1.0, \sigma_{\varepsilon} = 1.3$.

The following initial and boundary conditions were used:

$$-\text{at } \tau = 0 : \Psi(X,Y,0) = \Omega(X,Y,0) = K(X,Y,0) = E(X,Y,0) = \Theta(X,Y,0) = 0 \tag{6a}$$

$$-\text{at } Y = 0 : \Psi = 0,\ \frac{\partial \Psi}{\partial Y} = 0,\ \Omega = -\frac{\partial^2 \Psi}{\partial Y^2},\ \frac{\partial \Theta}{\partial Y} = \mathrm{N_{rad}} \cdot Q_{\mathrm{rad}},\ K = 0,\ \frac{\partial E}{\partial Y} = 0 \tag{6b}$$

$$-\text{at } Y = 1 : \Psi = 0,\ \frac{\partial \Psi}{\partial Y} = 0,\ \Omega = -\frac{\partial^2 \Psi}{\partial Y^2},\ \frac{\partial \Theta}{\partial Y} = \mathrm{N_{rad}} \cdot Q_{\mathrm{rad}},\ K = 0,\ \frac{\partial E}{\partial Y} = 0 \tag{6c}$$

$$-\text{at } X = 0 \text{ and } X = 1 : \Psi = 0,\ \frac{\partial \Psi}{\partial X} = 0,\ \Omega = -\frac{\partial^2 \Psi}{\partial X^2},\ \Theta = -0.5,\ K = 0,\ \frac{\partial E}{\partial X} = 0 \tag{6d}$$

$$-\text{at the heat source surface} : \Psi = 0,\ \frac{\partial \Psi}{\partial \overline{n}} = 0,\ \Omega = -\frac{\partial^2 \Psi}{\partial \overline{n}^2},\ \Theta = 0.5,\ K = 0,\ \frac{\partial E}{\partial \overline{n}} = 0 \tag{6e}$$

The thermal boundary conditions at the adiabatic walls must include the contribution of the dimensionless net radiative heat flux because of radiative exchanges among surfaces. To evaluate the effects of thermal radiation, the net radiative heat flux Q_{rad} can be determined, taking into account reflection effects, by the following equations:

$$Q_{\mathrm{rad},k} = R_k - \sum_{i=1}^{N} F_{k-i} R_i. \tag{7}$$

Here, indices "k" and "i" denote the individual surface elements and the ranges for these indices are from 1 till N.

The view factors F_{k-i} between the surface elements "k" and "i" are calculated by Hottel's crossed-string method (Miroshnichenko and Sheremet, 2015; Sheremet and Miroshnichenko, 2016; Martyushev and Sheremet, 2014a; Siegel and Howell, 2002). For diffusive gray and opaque internal surfaces, the radiosity R_k for all elements which are used is written in the following dimensionless form:

$$R_k = (1 - \tilde{\varepsilon}_k) \sum_{i=1}^{N} F_{k-i} R_i + \tilde{\varepsilon}_k (1 - \zeta)^4 \left(\Theta_k + 0.5 \frac{1 + \zeta}{1 - \zeta} \right)^4. \tag{8}$$

Here, $\zeta = T_c / T_h$ is the temperature parameter.

The average total Nusselt number has been defined as $\mathrm{Nu}_{\mathrm{total}} = \mathrm{Nu}_{\mathrm{con}}+\mathrm{Nu}_{\mathrm{rad}}$. It should be noted that average convective Nusselt number was defined as $\mathrm{Nu}_{\mathrm{con}} = \frac{L}{l_{hs}}\int_0^{l_{hs}/L}\left|\frac{\partial\Theta}{\partial X}\right|_{X=l/L}dY + \frac{L}{l_{hs}}\int_0^{l_{hs}/L}\left|\frac{\partial\Theta}{\partial Y}\right|_{Y=l_{hs}/L}dX + \frac{L}{l_{hs}}\int_0^{l_{hs}/L}\left|\frac{\partial\Theta}{\partial X}\right|_{X=(l+l_{hs})/L}dY$, while the average radiative Nusselt number can be defined as $\mathrm{Nu}_{\mathrm{rad}} = N_{\mathrm{rad}}\frac{L}{l_{hs}}\int_0^{l_{hs}/L}Q_{\mathrm{rad}}\Big|_{X=l/L}dY + N_{\mathrm{rad}}\frac{L}{l_{hs}}\int_0^{l_{hs}/L}Q_{\mathrm{rad}}\Big|_{Y=l_{hs}/L}dX + N_{\mathrm{rad}}\frac{L}{l_{hs}}\int_0^{l_{hs}/L}Q_{\mathrm{rad}}\Big|_{X=(l+l_{hs})/L}dY$.

3. Numerical method and validation

Before proceeding further, it is convenient to introduce a coordinate transformation in vector form mapping any point (X,Y) in the physical domain to the points (ξ,η) in the computational domain. This special algebraic transformation is used for thickening of the computational grid (Miroshnichenko and Sheremet, 2015; Kim and Viskanta, 1984):

$$\begin{cases} \xi = a + \dfrac{b-a}{2}\left\{1+\tan\left[\dfrac{\pi\kappa}{b-a}\left(X-\dfrac{a+b}{2}\right)\right]\Big/\tan\left[\dfrac{\pi}{2}\kappa\right]\right\}, \\ \eta = a + \dfrac{b-a}{2}\left\{1+\tan\left[\dfrac{\pi\kappa}{b-a}\left(Y-\dfrac{a+b}{2}\right)\right]\Big/\tan\left[\dfrac{\pi}{2}\kappa\right]\right\} \end{cases} \tag{9}$$

Here, a and b are the borders of the calculation domain for the considered coordinates, while κ is the deformation parameter. In the present study, $\kappa = 0.8$.

Taking into account this transformation, the governing equations (1)-(5) can be written as follows:

$$\frac{d^2\xi}{dX^2}\frac{\partial\Psi}{\partial\xi} + \left(\frac{d\xi}{dX}\right)^2\frac{\partial^2\Psi}{\partial\xi^2} + \frac{d^2\eta}{dY^2}\frac{\partial\Psi}{\partial\eta} + \left(\frac{d\eta}{dY}\right)^2\frac{\partial^2\Psi}{\partial\eta^2} = -\Omega, \tag{10}$$

$$\begin{aligned} &\frac{\partial\Omega}{\partial\tau} + \left(U - \frac{d\xi}{dX}\frac{\partial\nu_t}{\partial\xi}\right)\frac{d\xi}{dX}\frac{\partial\Omega}{\partial\xi} + \left(V - \frac{d\eta}{dY}\frac{\partial\nu_t}{\partial\eta}\right)\frac{d\eta}{dY}\frac{\partial\Omega}{\partial\eta} \\ &= \frac{d\xi}{dX}\frac{\partial}{\partial\xi}\left[\left(\sqrt{\frac{Pr}{Ra}}+\nu_t\right)\frac{d\xi}{dX}\frac{\partial\Omega}{\partial\xi}\right] + \frac{d\eta}{dY}\frac{\partial}{\partial\eta}\left[\left(\sqrt{\frac{Pr}{Ra}}+\nu_t\right)\frac{d\eta}{dY}\frac{\partial\Omega}{\partial\eta}\right] \\ &+ \left(\frac{d^2\xi}{dX^2}\frac{\partial\nu_t}{\partial\xi} + \left(\frac{d\xi}{dX}\right)^2\frac{\partial^2\nu_t}{\partial\xi^2} - \frac{d^2\eta}{dY^2}\frac{\partial\nu_t}{\partial\eta} - \left(\frac{d\eta}{dY}\right)^2\frac{\partial^2\nu_t}{\partial\eta^2}\right) \\ &\times\left(\Omega + 2\frac{d\eta}{dY}\frac{\partial U}{\partial\eta}\right) + 4\frac{d\xi}{dX}\left(\frac{d\eta}{dY}\right)^2\frac{\partial^2\nu_t}{\partial\xi\partial\eta}\frac{\partial V}{\partial\eta} + \frac{d\xi}{dX}\frac{\partial\Theta}{\partial\xi}, \end{aligned} \tag{11}$$

$$\frac{\partial \Theta}{\partial \tau} + U\frac{d\xi}{dX}\frac{\partial \Theta}{\partial \xi} + V\frac{d\eta}{dY}\frac{\partial \Theta}{\partial \eta} = \frac{d\xi}{dX}\frac{\partial}{\partial \xi}\left[\left(\frac{1}{\sqrt{Ra \cdot Pr}} + \frac{\nu_t}{Pr_t}\right)\frac{d\xi}{dX}\frac{\partial \Theta}{\partial \xi}\right] + \frac{d\eta}{dY}\frac{\partial}{\partial \eta}\left[\left(\frac{1}{\sqrt{Ra \cdot Pr}} + \frac{\nu_t}{Pr_t}\right)\frac{d\eta}{dY}\frac{\partial \Theta}{\partial \eta}\right], \tag{12}$$

$$\frac{\partial K}{\partial \tau} + U\frac{d\xi}{dX}\frac{\partial K}{\partial \xi} + V\frac{d\eta}{dY}\frac{\partial K}{\partial \eta} = \frac{d\xi}{dX}\frac{\partial}{\partial \xi}\left[\left(\sqrt{\frac{\mathrm{Pr}}{Ra}} + \frac{\nu_t}{\sigma_k}\right)\frac{d\xi}{dX}\frac{\partial K}{\partial \xi}\right] + \frac{d\eta}{dY}\frac{\partial}{\partial \eta}\left[\left(\sqrt{\frac{Pr}{Ra}} + \frac{\nu_t}{\sigma_k}\right)\frac{d\eta}{dY}\frac{\partial K}{\partial \eta}\right] + \overline{P}_k + \overline{G}_k - E, \tag{13}$$

$$\frac{\partial E}{\partial \tau} + U\frac{d\xi}{dX}\frac{\partial E}{\partial \xi} + V\frac{d\eta}{dY}\frac{\partial E}{\partial \eta} = \frac{d\xi}{dX}\frac{\partial}{\partial \xi}\left[\left(\sqrt{\frac{Pr}{Ra}} + \frac{\nu_t}{\sigma_\varepsilon}\right)\frac{d\xi}{dX}\frac{\partial E}{\partial \xi}\right] + \frac{d\eta}{dY}\frac{\partial}{\partial \eta}\left[\left(\sqrt{\frac{Pr}{Ra}} + \frac{\nu_t}{\sigma_\varepsilon}\right)\frac{d\eta}{dY}\frac{\partial E}{\partial \eta}\right] + c_{1\varepsilon}\left(\overline{P}_k + c_{3\varepsilon}\overline{G}_k\right)\frac{E}{K} - c_{2\varepsilon}\frac{E^2}{K} \tag{14}$$

Here, $\overline{P}_k = \nu_t\left[2\left(\frac{d\xi}{dX}\frac{\partial U}{\partial \xi}\right)^2 + 2\left(\frac{d\eta}{dY}\frac{\partial V}{\partial \eta}\right)^2 + \left(\frac{d\eta}{dY}\frac{\partial U}{\partial \eta} + \frac{d\xi}{dX}\frac{\partial V}{\partial \xi}\right)^2\right]$, $\overline{G}_k = -\frac{\nu_t}{\mathrm{Pr}_t}\frac{d\eta}{dY}\frac{\partial \Theta}{\partial \eta}$.

The corresponding initial and boundary conditions are given by:

– at $\tau = 0$:

$$\Psi(\xi, \eta, 0) = \Omega(\xi, \eta, 0) = \Theta(\xi, \eta, 0) = K(\xi, \eta, 0) = E(\xi, \eta, 0) = 0 \tag{15a}$$

– at $\eta = 0$:

$$\Psi = 0,\ \frac{\partial \Psi}{\partial \eta} = 0,\ \Omega = -\left(\frac{d\eta}{dY}\right)^2\frac{\partial^2 \Psi}{\partial \eta^2},\ \frac{d\eta}{dY}\frac{\partial \Theta}{\partial \eta} = \mathrm{N_{rad}} \cdot Q_{\mathrm{rad}},\ K = 0,\ \frac{\partial E}{\partial \eta} = 0 \tag{15b}$$

– at $\eta = 1$:

$$\Psi = 0,\ \frac{\partial \Psi}{\partial \eta} = 0,\ \Omega = -\left(\frac{d\eta}{dY}\right)^2\frac{\partial^2 \Psi}{\partial \eta^2},\ \frac{d\eta}{dY}\frac{\partial \Theta}{\partial \eta} = -\mathrm{N_{rad}} \cdot Q_{\mathrm{rad}},\ K = 0,\ \frac{\partial E}{\partial \eta} = 0 \tag{15c}$$

– at $\xi = 0$ and $\xi = 1$:

$$\Psi = 0,\ \frac{\partial \Psi}{\partial \xi} = 0,\ \Omega = -\left(\frac{d\xi}{dX}\right)^2\frac{\partial^2 \Psi}{\partial \xi^2},\ \Theta = -0.5,\ K = 0,\ \frac{\partial E}{\partial \xi} = 0 \tag{15d}$$

– at the heat source surface:

$$\Psi = 0,\ \frac{\partial \Psi}{\partial \overline{n}} = 0,\ \Omega = -\left(\frac{d\overline{n}}{d(X,Y)}\right)^2 \frac{\partial^2 \Psi}{\partial \overline{n}^2},\ \Theta = 0.5,\ K = 0,\ \frac{\partial E}{\partial \overline{n}} = 0 \tag{15e}$$

The finite difference method was used to solve the formulated partial differential equations (10)-(14) with corresponding initial and boundary conditions equation (15). The Poisson equation for the stream function equation (10) was discretized at each grid-point. This procedure is based on the standard five-point discretization for second derivatives with second-order truncation error. The successive over relaxation method was applied to solve the obtained system of linear equations. The strategy used to solve the remaining governing equations (11)-(14) including the two additional transport equations for the turbulence kinetic energy and the turbulence dissipation rate is locally one-dimensional method of A.A. Samarskii (Miroshnichenko and Sheremet, 2015; Sheremet and Miroshnichenko, 2016; Martyushev and Sheremet, 2014a, 2014b; Samarskii, 1977). An approximation of the convective terms is based on Samarskii's monotonic scheme. Second-order central difference scheme is used for an approximation of the diffusion terms. The discretization of parabolic equations leads to a tridiagonal linear system, which is solved by the Thomas algorithm.

The independence of the solution with respect to the grid size has been studied for a Rayleigh number of 10^9. Four different grid sizes of 50×50, 100×100, 150×150 and 200×200 points have been used. Figure 2 shows an influence of the mesh parameters on the average convective and radiative Nusselt numbers. On the basis of this analysis, a grid of 150×150 points has been selected for the following detailed study.

To validate the numerical model, a comparison was made with experimental data of Ampofo and Karayiannis's (2003) study for turbulent natural convection in a square cavity without heat source. A fairly good agreement with the experimental results is observed in Figure 3.

4. Results and discussion

The effect of heat source location on heat transfer by natural convection and thermal radiation has been performed using numerical techniques. The influence of Ra and $\tilde{\varepsilon}$ has been also investigated. The present results have been obtained for a wide range of both the

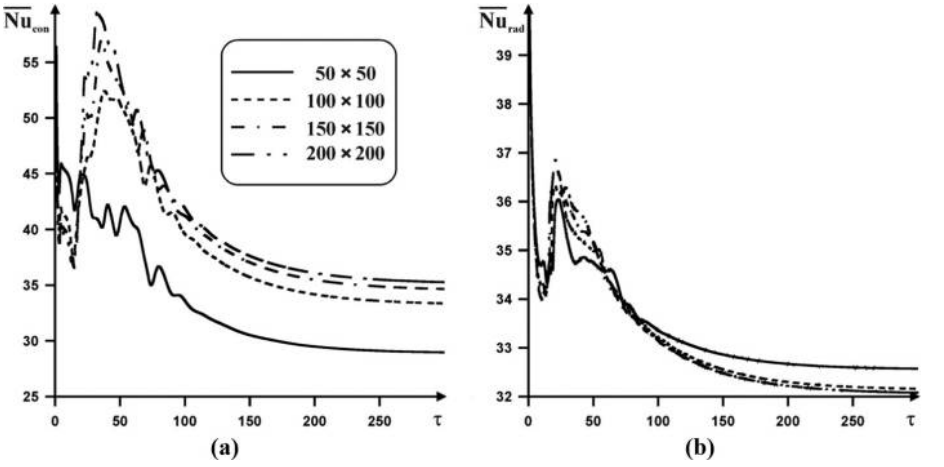

Figure 2.
Variation of the average convective (a) and radiative (b) Nusselt numbers at the left vertical wall

Rayleigh numbers from 10^8 to 10^{10} and surface emissivity from 0 to 0.9, and for different locations of the heat source $0.2 \leq l/L \leq 0.4$ at $Pr = 0.7$.

An evolution of the thermal plume over the heat source is shown in Figure 4. The heat source of finite sizes is located on the bottom wall of the cavity. It is worth noting that at the beginning of the process, two thermal plumes are formed in the upper corners of the heat source. Such behavior defines a formation of ascending convective flows close to the vertical walls of the heater with boundary layers separation in the upper corners of the heat source. At the same time, one can find a penetration of low temperature waves from the vertical walls of the cavity to the heater surface. Taking into account a presence of a huge cooling surface in comparison with a heat source surface, one can find a further cooling of the cavity from these walls. Further cooling of the cavity leads to a formation of steady-state regime to the moment $\tau = 300$.

It is well known that the Rayleigh number reflects a formation of different modes of fluid flow and heat transfer during natural convection within the enclosures. Figure 5 shows streamlines and isotherms for different values of Ra at $\tilde{\varepsilon} = 0.6$, $l/L = 0.2$. The fluid rises along the vertical sides of the local heater due to the buoyancy force impact, while the fluid falls along each cold vertical wall of the cavity. Such behavior reflects a formation of a counterclockwise vortex in the left part of the cavity and clockwise vortex in the right part of the cavity. Therefore, two convective cells are generated around the heat source. It is clear that the location of the heater near left wall can lead to an increase in the size of one cell to the detriment of other one. Two counterclockwise vortices are formed in the left part of the cavity at $Ra = 10^8$. Nevertheless, an intensity of these cells is negligible in comparison with the main clockwise cell. It should be noted that an increase in the Rayleigh number leads to a combination of these two cells in one more intensive vortex because of an essential effect of the buoyancy force. At the same time, this combined counterclockwise cell for high Ra begins to deform the main vortex that results in an attenuation of the main vortex. The distribution of isotherms in the cavity is significantly distorted with Ra. The shape of the thermal plume is similar to the boundary between counterclockwise and clockwise vortices within the cavity. An increase in Rayleigh number leads to both an essential intensification of convective flow and a decrease in the thermal boundary layers thickness close to the vertical walls.

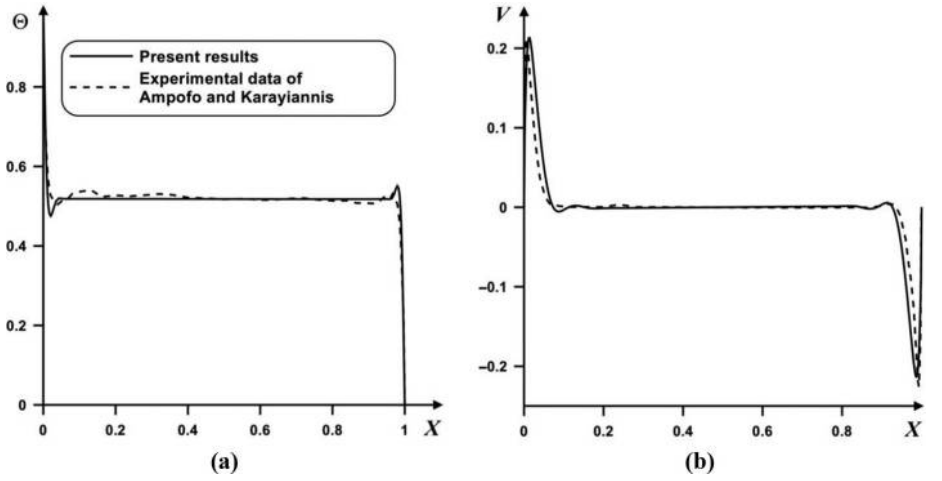

Figure 3.
The temperature profiles (a) and vertical velocity profiles (b) at $Ra = 1.58 \cdot 10^9$ in comparison with the experimental data of Ampofo and Karayiannis (2003)

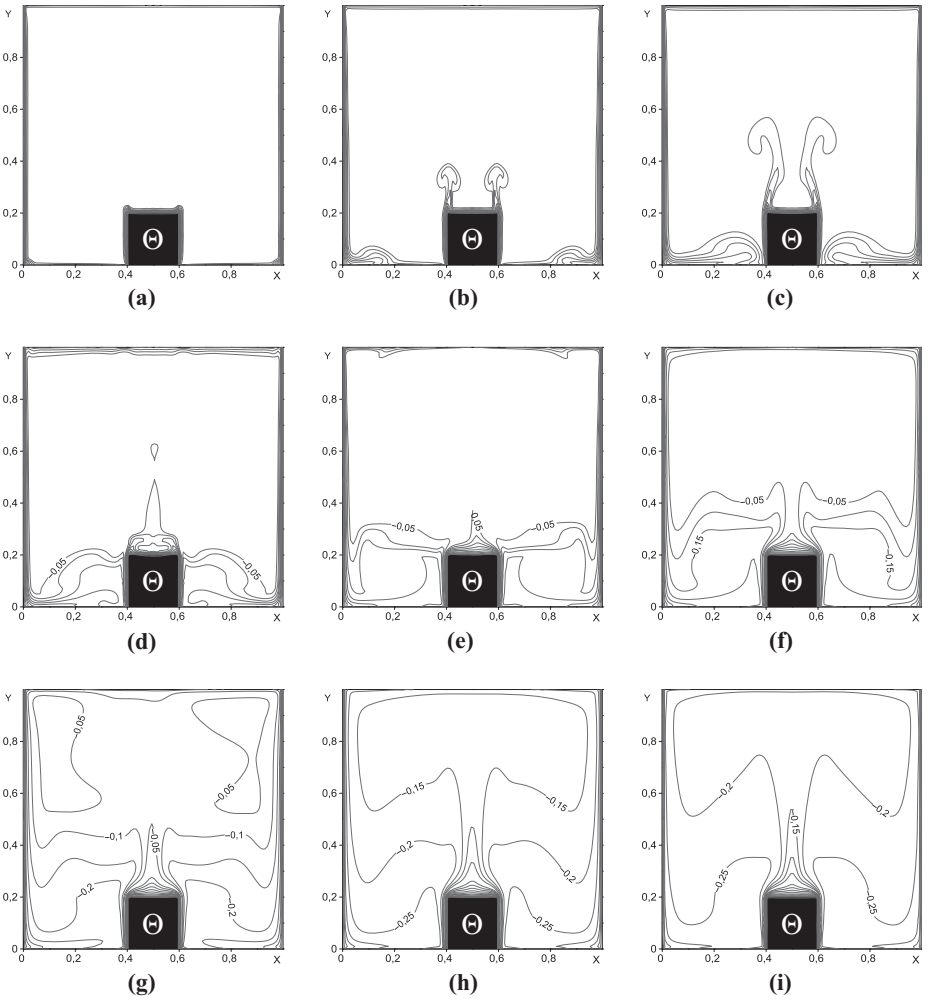

Figure 4.
Evolution of isotherms with time at $Ra = 10^{10}$, $\tilde{\varepsilon} = 0.6$ and $l/L = 0.4$

Notes: (a) $\tau = 1$; (b) $\tau = 3$; (c) $\tau = 5$; (d) $\tau = 10$; (e) $\tau = 20$; (f) $\tau = 30$; (g) $\tau = 50$; (h) $\tau = 100$; (i) $\tau = 300$

The average total Nusselt number with time at the heat source surface for different *Ra* is shown in Figure 6. It should be noted that the increasing effect of the buoyancy force leads to an increase in the heat transfer rate. Such behavior can be explained by an intensification of convective and radiative heat transfer modes. In particular, the total Nusselt number at $Ra = 10^{10}$ is greater than this value at $Ra = 10^{8}$ up to 3.9 times. Also, it is worth noting that an essential effect of time on the heat transfer rate is for $\tau < 100$ that can be explained by a formation of different levels of heat transfer such as heat conduction at the beginning of the process, convective cooling of the cavity and steady-state regime reflecting equality of heat input from the heater and heat output to the cold walls.

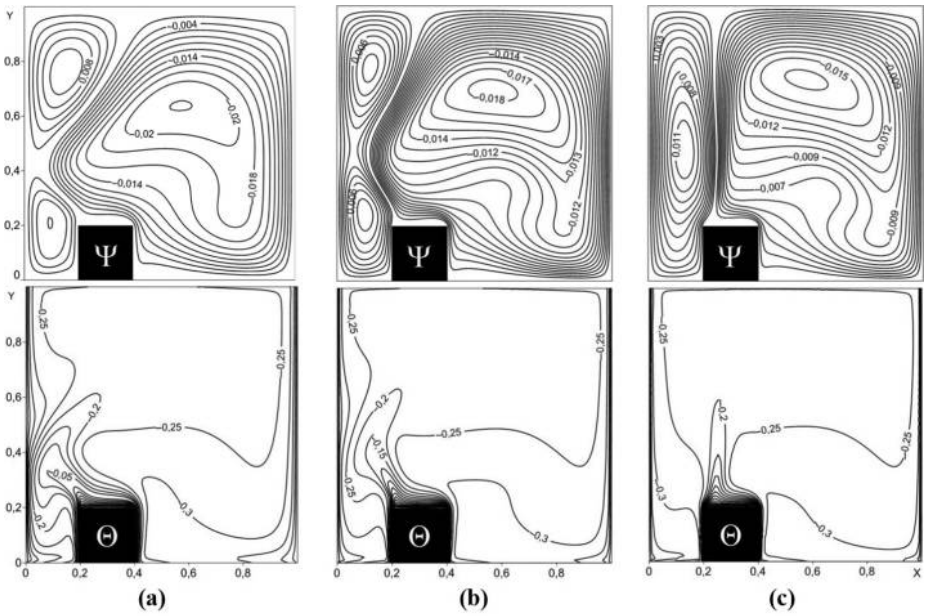

Notes: (a) $Ra = 10^8$; (b) $Ra = 10^9$; (c) $Ra = 10^{10}$

Figure 5.
Streamlines Ψ and isotherms Θ at $\tilde{\varepsilon} = 0.6$, $\tau = 300$ and $l/L = 0.2$

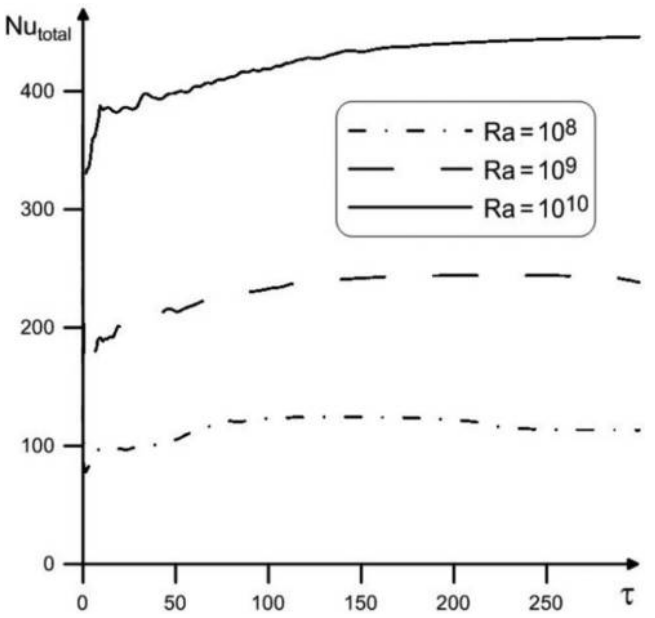

Figure 6.
Variation of the average total Nusselt number at the heat source surface with dimensionless time and Rayleigh number at $l/L = 0.2$ and $\tilde{\varepsilon} = 0.6$

Figure 7 shows isolines of stream function and temperature at $Ra = 10^{10}$, $\tau = 300$ and $l/L = 0.2$ for different values of the surface emissivity. It should be noted that in the case without radiation effects, the surface emissivity is equal to zero. In the case of radiation interaction, an increase in $\tilde{\varepsilon}$ leads to a weak intensification of convective flow in the cavity, e.g. $|\Psi|_{\max}^{\tilde{\varepsilon}=0.3} = 0.0144$, $|\Psi|_{\max}^{\tilde{\varepsilon}=0.6} = 0.0162$ and $|\Psi|_{\max}^{\tilde{\varepsilon}=0.9} = 0.0175$. Primary single convective cell with clockwise motion can be identified as the main convective structure inside the cavity. At the same time, size of counterclockwise cell decreases with $\tilde{\varepsilon}$. Moreover, an increase in the surface emissivity leads to a displacement of the secondary convective cell core close to the bottom wall with attenuation of this circulation. Also, one can find more intensive cooling of the cavity with $\tilde{\varepsilon}$ because of an intensification of additional heat transfer mechanism in diathermal medium.

Figure 8 shows an evolution of Nu_{total} at different values of the surface emissivity. At $\tau = 300$, the average total Nusselt number increases up to 3.56 times at changing of $\tilde{\varepsilon}$ from 0 to 0.9. It should be noted that an increase in the surface emissivity leads to a reduction of convective heat transfer rate and an increase in the radiative heat transfer rate because of an increase in the net radiative heat flux. Therefore, Nu_{total} is an increasing function of surface emissivity.

The effect of a heater location on heat and fluid flow is studied by varying location as shown in Figure 9. For all numerical results, the ratio of the heat source size (l_{hs}/L) is taken 0.2. Regardless of the considered heat source location, two convective cells are formed inside the cavity. These vortices define clockwise and counterclockwise fluid motion in the left and right parts of the cavity relative to the heater. It is observed that a decrease in l/L leads to an increase in the size of the right convective cell to the detriment of other one. In particular, it

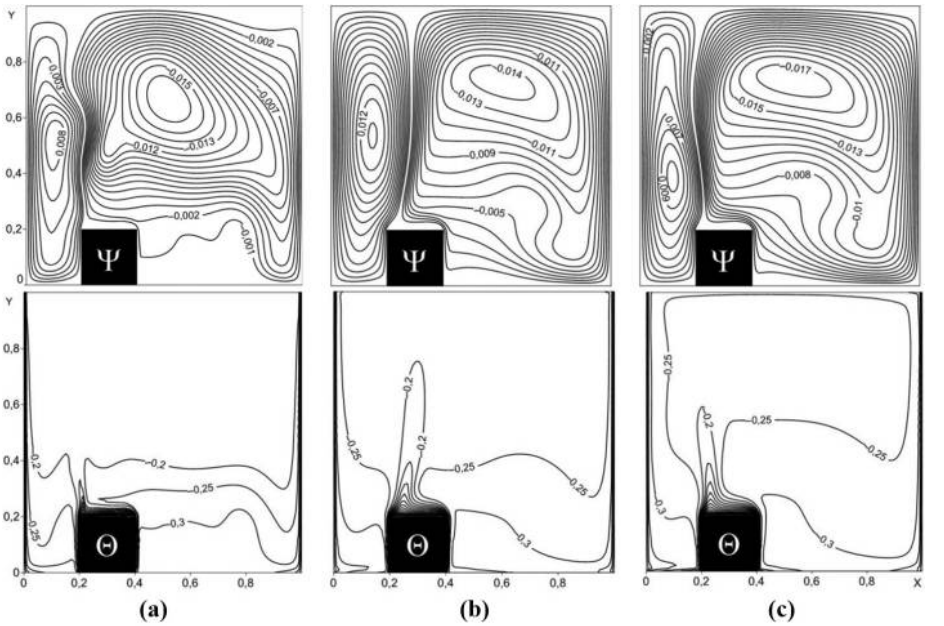

Figure 7.
Streamlines Ψ and isotherms Θ at $Ra = 10^{10}$, $\tau = 300$ and $l/L = 0.2$

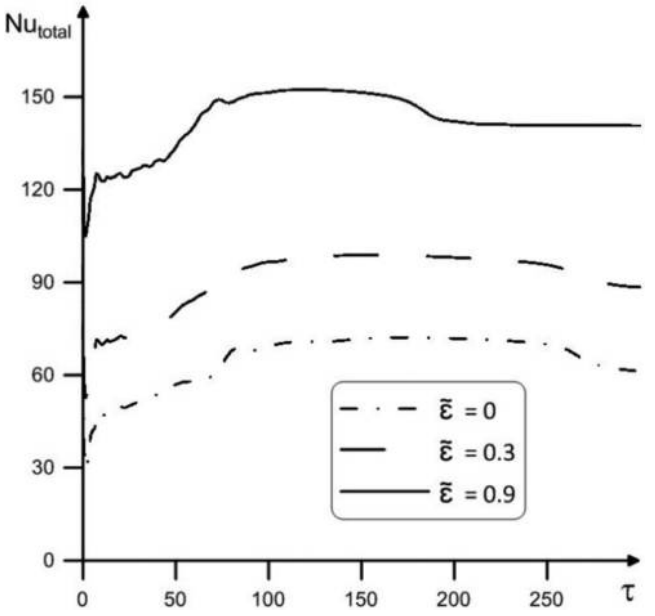

Figure 8.
Evolution of the average total Nusselt number at the heat source surface with surface emissivity at $Ra = 10^{10}$ and $l/L = 0.2$

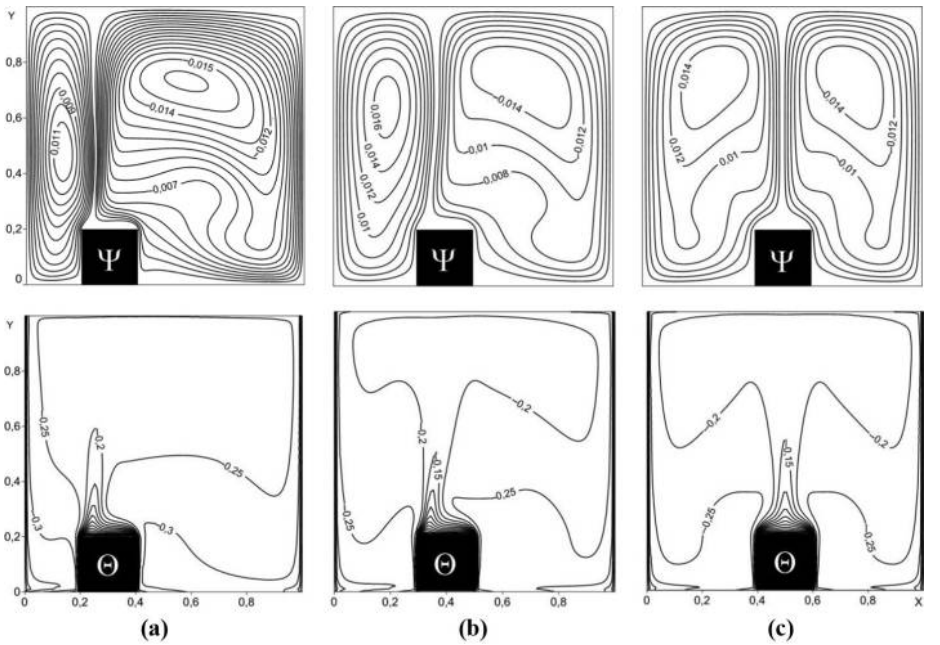

Figure 9.
Streamlines Ψ and isotherms Θ at $Ra = 10^{10}$, $\tau = 300$ and $\tilde{\varepsilon} = 0.6$

Notes: (a) $l/L = 0.2$; (b) $l/L = 0.3$; (c) $l/L = 0.4$

was found that an intensity of the right convective cell increases with displacement of the heater close to the left wall $|\Psi|_{\max}^{l/L=0.4} = 0.0158 < |\Psi|_{\max}^{l/L=0.3} = 0.0159 < |\Psi|_{\max}^{l/L=0.2} = 0.0162$. These results indicate that a shift of the heater from the middle position leads to change of the intensity of convective flows within the cavity.

The effect of the heater location on profiles of the temperature at the cross-section $Y = 0.5$ is presented in Figure 10. It should be noted that an increase in l/L leads to an increase in the temperature close to the left and right vertical walls.

Such behavior can be explained by more intensive influence of cooling wall on the heat source that obstructs a heating of the cavity in more essential style in comparison with, for example, central position of the heater. The maximum dimensionless temperature is obtained for the case when the heat source is located in center of the bottom wall.

A quantitative analysis was also carried out for the average Nusselt number. Figure 11 shows the effect of the heat source position on the average total Nusselt number. It can be seen from this figure that a displacement of the heater close to the left wall leads to an increase in the heat transfer rate because of an essential increase in the temperature gradient near the cooling wall. For instance, at $\tau = 300$ the average total Nusselt numbers for $l/L = 0.4$, $l/L = 0.3$ and $l/L = 0.2$ were 427.4, 432.2 and 445.7, respectively.

5. Conclusions

Combined heat transfer of natural convection and thermal radiation in a square cavity with a heat source has been studied numerically. Detailed analysis has been carried out to understand the effect of various locations of the heat source on heat transfer and fluid flow parameters. An efficient numerical technique has been developed to solve this problem. We can conclude that the presence of surface radiation leads to both an increase in the average total Nusselt number and intensive cooling of such type of

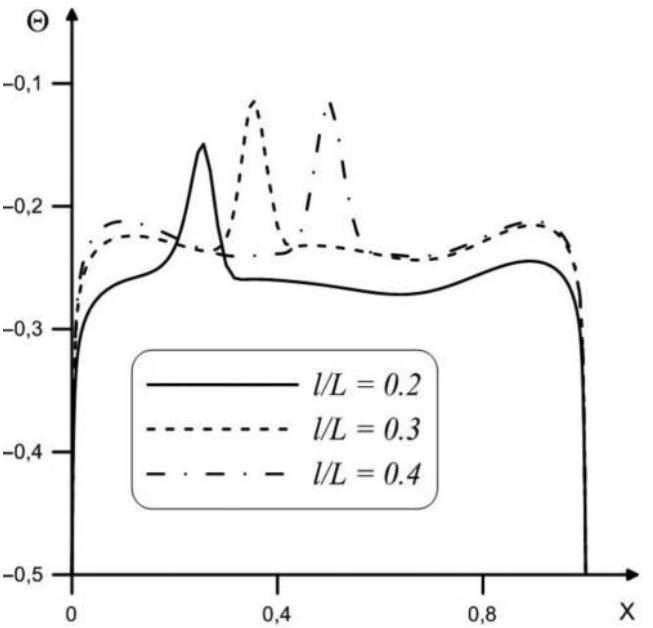

Figure 10.
Temperature profiles at $Y = 0.5$ for $Ra = 10^{10}$, $\tilde{\varepsilon} = 0.6$ and $\tau = 300$ and different values of the heat source location

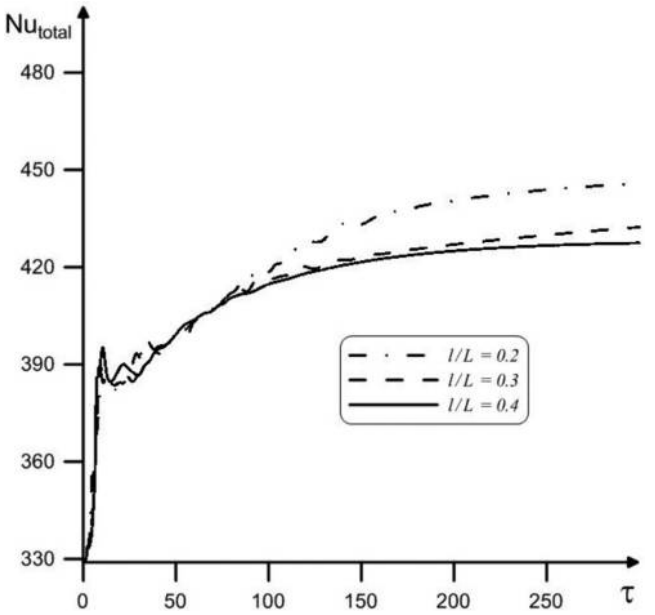

Figure 11.
Evolution of the average total Nusselt number at the heat source surface with heat source location at $Ra = 10^{10}$ and $\bar{\varepsilon} = 0.6$

system. A significant intensification of convective flow was also observed owing to an increase in Rayleigh number. It should be noted that a displacement of the heater from central part of the bottom wall leads to significant modification of the thermal plume and flow pattern inside the cavity. Furthermore, the average total Nusselt number is a decreasing function of l/L. From design point of view for cooling of considered area, one should not ignore the location of heat source which plays an essential role in heat transfer process.

References

Ampofo, F. and Karayiannis, T.G. (2003), "Experimental benchmark data for turbulent natural convection in an air filled square cavity", *International Journal of Heat and Mass Transfer*, Vol. 46 No. 19, pp. 3551-3572.

Biswas, N., Mahapatra, P.S., Manna, N.K. and Roy, P.C. (2016), "Influence of heater aspect ratio on natural convection in a rectangular enclosure", *Heat Transfer Engineering*, Vol. 37 No. 2, pp. 125-139.

Colomer, G., Costa, M., Consul, A. and Oliva, R. (2004), "Three-dimensional numerical simulation of convection and radiation in a differentially heated cavity using the discrete ordinates method", *International Journal of Heat and Mass Transfer*, Vol. 47 No. 2, pp. 257-269.

Diaz, G. and Winston, R. (2008), "Effect of surface radiation on natural convection in parabolic enclosures", *Numerical Heat Transfer A*, Vol. 53 No. 9, pp. 891-906.

Fusegi, T. and Farouk, B. (1989), "Laminar and turbulent natural convection-radiation interactions in a square enclosure filled with a non-gray gas", *Numerical Heat Transfer A*, Vol. 15 No. 3, pp. 303-322.

Ibrahim, A., Saury, D. and Lemonnier, D. (2013), "Coupling of turbulent natural convection with radiation in an air-filled differentially-heated cavity at Ra = 1.5·109", *Computers & Fluids*, Vol. 88, pp. 115-125.

Jaluria, Y. (1998), *Design and Optimization of Thermal Systems*, McGraw-Hill, New York.

Kim, D.M. and Viskanta, R. (1984), "Study of the effects of wall conductance on natural convection in differentially oriented square cavities", *Journal of Fluid Mechanics*, Vol. 144 No. 1, pp. 153-176.

Launder, B.E. and Spalding, D.B. (1974), "The numerical computation of turbulent flows", *Computer Methods in Applied Mechanics and Engineering*, Vol. 3 No. 2, pp. 269-289.

Martyushev, S.G. and Sheremet, M.A. (2014a), "Conjugate natural convection combined with surface thermal radiation in an air filled cavity with internal heat source", *International Journal of Thermal Sciences*, Vol. 76, pp. 51-67.

Martyushev, S.G. and Sheremet, M.A. (2014b), "Conjugate natural convection combined with surface thermal radiation in a three-dimensional enclosure with a heat source", *International Journal of Heat and Mass Transfer*, Vol. 73, pp. 340-353.

Mezrhab, A., Bouali, H., Amaoui, H. and Bouzidi, M. (2006), "Computation of combined natural-convection and radiation heat-transfer in a cavity having a square body at its center", *Applied Energy*, Vol. 83 No. 9, pp. 1004-1023.

Miroshnichenko, I.V. and Sheremet, M.A. (2015), "Numerical simulation of turbulent natural convection combined with surface thermal radiation in a square cavity", *International Journal of Numerical Methods for Heat & Fluid Flow*, Vol. 25 No. 7, pp. 1600-1618.

Paroncini, M. and Corvaro, F. (2009), "Natural convection in a square enclosure with a hot source", *International Journal of Thermal Sciences*, Vol. 48 No. 9, pp. 1683-1695.

Samarskii, A.A. (1977), *Theory of Difference Schemes*, Nauka, Moscow.

Saravanan, S. and Sivaraj, C. (2014), "Surface radiation effect on convection in a closed enclosure driven by a discrete heater", *International Communications in Heat and Mass Transfer*, Vol. 53, pp. 34-38.

Sezai, I. and Mohamad, A.A. (2000), "Natural convection from a discrete heat source on the bottom of a horizontal enclosure", *International Journal of Heat and Mass Transfer*, Vol. 43 No. 13, pp. 2257-2266.

Sharma, A.K., Velusamy, K., Balaji, C. and Venkateshan, S.P. (2007), "Conjugate turbulent natural convection with surface radiation in air filled rectangular enclosures", *International Journal of Heat and Mass Transfer*, Vol. 50 Nos 3/4, pp. 625-639.

Shati, A.K.A., Blakey, S.G. and Beck, S.B.M. (2013), "An empirical solution to turbulent natural convection and radiation heat transfer in square and rectangular enclosures", *Applied Thermal Engineering*, Vol. 51 Nos 1/2, pp. 364-370.

Sheremet, M.A. and Miroshnichenko, I.V. (2015), "Numerical study of turbulent natural convection in a cube having finite thickness heat-conducting walls", *Heat and Mass Transfer*, Vol. 51 No. 11, pp. 1559-1569.

Sheremet, M.A. and Miroshnichenko, I.V. (2016), "Effect of surface radiation on transient natural convection in a wavy-walled cavity", *Numerical Heat Transfer A*, Vol. 69 No. 4, pp. 369-382.

Siegel, R. and Howell, J.R. (2002), *Thermal Radiation Heat Transfer*, Taylor & Francis, London.

Singh, D.K. and Singh, S.N. (2015), "Conjugate free convection with surface radiation in open top cavity", *International Journal of Heat and Mass Transfer*, Vol. 89, pp. 444-453.

Sun, H., Chenier, E. and Lauriat, G. (2011), "Effect of surface radiation on the breakdown of steady natural convection flows in a square, air-filled cavity containing a centered inner body", *Applied Thermal Engineering*, Vol. 31 Nos 6/7, pp. 1252-1262.

Wu, T. and Lei, C. (2015), "On numerical modelling of conjugate turbulent natural convection and radiation in a differentially heated cavity", *International Journal of Heat and Mass Transfer*, Vol. 91, pp. 454-466.

Xaman, J., Arcea, J., Alvarez, G. and Chaveza, Y. (2008), "Laminar and turbulent natural convection combined with surface thermal radiation in a square cavity with a glass wall", *International Journal of Thermal Sciences*, Vol. 47 No. 12, pp. 1630-1638.

Corresponding author
Mikhail Sheremet can be contacted at: Michael-sher@yandex.ru